The Journal of Adhesion

Effect of Curing Pressure on the Strength of Adhesively Bonded Joints

Murat Demir Aydın[a]; Şemsettın Temiz[b]; Adnan Özel[b]

[a] Erzurum MYO, Atatürk Üniversity, Erzurum, Turkey [b] Faculty of Engineering, Atatürk Üniversity, Erzurum, Turkey

PLEASE SCROLL DOWN FOR ARTICLE

Taylor & Francis
Taylor & Francis Group

Effect of Curing Pressure on the Strength of Adhesively Bonded Joints

Murat Demir Aydın
Erzurum MYO, Atatürk Üniversity, Erzurum, Turkey

Şemsettın Temiz
Adnan Özel
Faculty of Engineering, Atatürk Üniversity, Erzurum, Turkey

It is important to be able to predict the mechanical response of adhesively bonded joints. To succeed in this, the accurate simulation of the behavior of adhesively bonded joints is an essential requirement because of the strain rate, temperature, and hydrostatic sensitivity of adhesive properties, which should be taken into consideration when developing a material model [1–11]. On the other hand, the load capabilities of adhesively bonded joints are affected by both applied pressure and temperature during cure. For this reason, in this study, the tensile load capabilities of single lap joints (SLJs) bonded with a flexible adhesive that possesses pressure-sensitive properties were experimentally investigated with respect to the applied pressure during the curing operation, and the experimental results were compared with finite element analysis (FEA) results. Finally, in addition to other parameters, such as the dependence on strain rate and the lack of yield criteria of adhesives, it was seen that the residual thermal stresses that occurred as a result of the applied pressure during the curing process at elevated temperature need to be taken into consideration to accurately simulate the mechanical behavior of adhesively bonded joints.

1. INTRODUCTION

Adhesive bonding is increasingly being selected as a joining method for high-performance applications and new uses are being made of

flexible adhesives in structural roles. Flexible adhesives, character-
ized by low glass-transition temperatures, low modulus, and large
strains to failure in comparison with structural adhesives such as
epoxies, are used extensively in nonstructural applications such as
footwear bonding, packaging, and sealing, where the adhesive is often
required to retain joint integrity during large deformations of the
adherends. Such applications have rarely required sophisticated pre-
dictive design calculations. However, the advantageous properties of
flexible adhesives in sustaining large strains and more evenly distri-
buting peel forces on the bonded substrates has led to their use for
structural joining applications. Their adoption in industries such as
the automotive industry, where design simulation is used extensively,
has driven the need to improve the understanding of the mechanical
properties of these adhesives [1–4].

Safe and reliable design of bonded structures is dependent on the
availability of reliable materials models and failure criteria that can
be used to predict the failure behavior of adhesively bonded struc-
tures. Also, temperature changes in adhesively bonded joints cause a
wide variety of different stress states because of the mismatch of the
adherends or to adhesive contraction by temperature or cure, as stated
by Adams *et al.* [5]. Currently, there are no well-established design
procedures for predicting failure behavior or relating changes in
material and geometric parameters to joint strength of bonded struc-
tures [1–12].

Many researchers have investigated the effects of adherends, the
thermal characteristics of single-lap joints (SLJs), and hygrothermal
effect of resin on the joints, some of which are mentioned here.

Harrison and Harrison developed a simple method for calculating
stresses near the ends of a parallel-sided adhesive layer and investi-
gated the stress concentration induced by residual thermal stresses
[13]. Cho and Lee studied the thermal and dimensional effects on
cocured composite/steel joints, considering the thermal degradation
of the resin [14]. Kim and coworkers investigated the stresses occur-
ring in an adhesively bonded tubular SLJ, considering the nonlinear
adhesive properties and thermal residual stresses due to fabrication,
and presented a failure model [15,16]. Cho *et al.* studied the effect of
curing temperature on the adhesion strength of polyamideimide/
copper joints and showed that adhesion strength decreased as the
thermal stress increased with the increase of both curing temperature
and time [17]. Humfeld and Dillard investigated thermal cycling
effects on the residual stresses in viscoelastic polymeric materials
bonded to stiff elastic substrates [18]. The residual stresses in the
elastic–viscoelastic bimaterial system incrementally shifted over time

when subjected to thermal cycling, and damaging tensile axial and peel stresses developed over time because of visco-elastic response to thermal stresses induced in the polymeric layer.

The residual thermal stresses affecting the strength of a joint generally occur as a result of different thermal properties between the adhesive and the adherend during the curing process at elevated temperature [5,19]. The importance of these stresses increases when the pressure applied for curing of the adhesives is taken into consideration [20]. In the present study, the tensile load capabilities of SLJs bonded with a flexible adhesive were experimentally investigated with respect to the applied pressure during the curing operation and compared with finite element analysis (FEA) results.

2. MECHANICAL CHARACTERIZATION OF ADHESIVE AND DATA REQUIREMENTS FOR A NONLINEAR STRESS ANALYSIS

The epoxy/acrylic hybrid adhesive used in this study is structural bonding tape (SBT) 9244 (produced by 3 M Company, St. Paul, MN, USA), which possesses pressure-sensitive and visco-elastic properties. The adhesive exhibits a nonlinear relationship between stress and strain. Hence, for the purpose of finite element analysis, elastic–plastic models have been used to describe the deformation behavior.

The onset of nonlinearity in the stress–strain curve is due to plastic deformation and occurs at the first yield stress. The subsequent increase in stress with strain is related to the effects of strain hardening, and stress calculations involve the use of a yield criterion. The most commonly used elastic–plastic model is based on the von Mises yield criterion, but it is known that the von Mises criterion is not an accurate description of yielding in adhesives where plasticity is sensitive to the hydrostatic component of stress as well as the shear component. For this reason, a pressure-dependent yield criterion is often used [1–4]. Drucker–Prager [21] and Raghava [22] criteria both account for hydrostatic pressure sensitivity in materials. In the study, the Raghava criterion, given as follows, was used:

$$(\sigma_1 - \sigma_2)^2 + (\sigma_2 - \sigma_3)^2 + (\sigma_3 - \sigma_1)^2 + 2 \cdot (|\sigma_c| - \sigma_t) \cdot (\sigma_1 + \sigma_2 + \sigma_3)$$
$$= 2 \cdot |\sigma_c| \cdot \sigma_t, \tag{1}$$

where σ_1, σ_2, and σ_3 are the principal stresses and σ_c and σ_t are

the compression and tensile strength. This criterion can be written differently:

$$q^2 + 3\sigma_t(\lambda - 1)\sigma_m = \lambda \cdot \sigma_t^2, \tag{2}$$

$$\lambda = \frac{\sigma_c}{\sigma_t}, \qquad \sigma_m = \frac{J_1}{3}.$$

q is the von Mises equivalent stress, expressed by

$$q^2 = \frac{1}{2}(\sigma_1 - \sigma_2)^2 + (\sigma_2 - \sigma_3)^2 + (\sigma_3 - \sigma_1)^2 = 3J_2, \tag{3}$$

where λ and J_1 are the ratio of the yield stress in compression to the yield stress in tension corresponding to the same equivalent plastic strain ($\bar{\varepsilon}^{pl}$) and the first invariant of the stress tensor, respectively. J_2 is the second invariant of the deviatoric stress tensor. The Raghava criterion exists in finite-element package ANSYS 10.0 (ANSYS Inc., Canonsburg, PA, USA) [23] as the "extended Drucker–Prager" model and is described by Eq. (4):

$$q^b + \alpha\sigma_m = \sigma_y^b(\bar{\varepsilon}^{pl}), \tag{4}$$

where α, σ_m, and $\sigma_y(\bar{\varepsilon}^{pl})$ are the material parameters referring to the pressure-sensitive parameter, the mean or hydrostatic stress, and the yield stress of the material, respectively. Also, b is the material parameter characterizing the shape of the yield surface. By assuming the special case of $b = 2$, rearranging, and comparing with Eq. (2), the following relationship for α can be derived:

$$\alpha = 3\sigma_t(\lambda - 1). \tag{5}$$

The data needed for this elastic–plastic model are E_a (elasticity modulus of adhesive), ν_e (Poisson's ratio), α, ψ (dilation angle), and $\sigma_y(\bar{\varepsilon}^{pl})$. The dilation angle ($\psi$) describes the orientation of the plastic flow

TABLE 1 Material Properties of the Adherend and Adhesives

Property	AA2024-T3 alloy	SBT 9244 adhesive	FM 73 adhesive [27–29]
E_a (MPa)	71875	81.86	2273.7
ν_e	0.33	0.35	0.35
σ_t (MPa)	482	20.96	70.84
ε_t (mm/mm)	0.1587	0.9449	0.548

Note. E_a: Young's modulus; ν_e: Poisson's ratio; σ_t: ultimate tensile strength; ε_t: ultimate tensile strain.

TABLE 2 Material Parameters for the Exponent Drucker–Prager Model (SBT 9244)

$\sigma_y(\bar{\varepsilon}^{pl})$	λ	α (Eq. 5)	$\tan \psi$ (Eq. 6)
See Fig. 1a	1.541	29.01	0.516

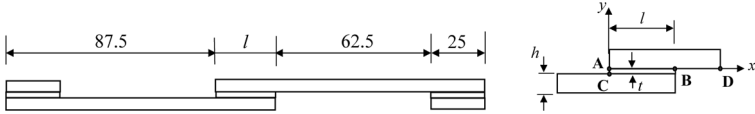vectors, and this is calculated from the plastic component of Poisson's ratio, ν_p, given as follows [1–4]:

$$\tan \psi = \frac{3(1 - 2\nu_p)}{2(1 + \nu_p)}. \tag{6}$$

Furthermore, the stress–strain behaviors of adhesives under shear, tension, or compression are necessary for the elastic–plastic stress analysis mentioned previously *via* nonlinear finite-element modeling (FEM). The properties of the adhesive required for finite-element analysis (FEA) have been determined from tensile and shear tests reported earlier. A fuller discussion can be found elsewhere [24–26]. Finally, the material properties of the adherend and adhesives are given in Table 1. Also, the exponent Drucker–Prager (Raghava) material constants (E_a, ν_e, ν_p, α, and ψ) are calculated and shown in Table 2.

3. PRODUCTION AND NUMERICAL MODELING OF SINGLE LAP JOINTS (SLJs)

3.1. Production of SLJs

SLJs shown in Table 3 were made of AA2024-T3 aluminum plate (Kastens & Knauer GMBH, Lilienthal, Germany) bonded using the film-type adhesive (SBT 9244). To assess the effects of both curing pressure and geometrical parameters on the performance of the SLJs, three different adherend thicknesses (1.6, 3.2, and 4.8 mm) and four overlap lengths (12.5, 25, 50, and 100 mm) were used for 0.5-MPa curing pressure, whereas three different adherend thicknesses (1.6, 3.2, and 4.8 mm) and two overlap lengths (25 and 100 mm) were used for 0.1-MPa curing pressure. Before bonding, the adherend surfaces (AA2024-T3) were degreased with acetone, sand blasted, etched with $H_2SO_4 + Na_2Cr_2O_7.2H_2O$ for 30 min at 60–65°C, washed in running tap water, and dried in an oven for 30 min at 60°C. Then, adhesive bonding with SBT 9244 was achieved by curing at 145°C in a hot press for 45 min. To observe the effect of curing pressure, two different

TABLE 3 Geometrical Parameters of the SLJs Used in Experimental and Numerical Studies (All Dimensions in mm)

Adhesive thickness t	Adherend width	Adherend thickness h	Overlap length l
0.17	25	1.6	12.5
		3.2	25
		4.8	50
			100

curing pressures were applied (0.1 and 0.5 MPa), as mentioned previously.

3.2. NonLinear Finite Element Modeling of SLJs

The stress analyses for the SLJs using a nonlinear finite element method were performed by considering the geometrical nonlinearity and nonlinear material behaviors based on the uniaxial tensile stress–strain behaviors (Figures 1a and 1b) of adhesive (SBT 9244) and adherend (AA2024-T3). Therefore, the ANSYS finite-element
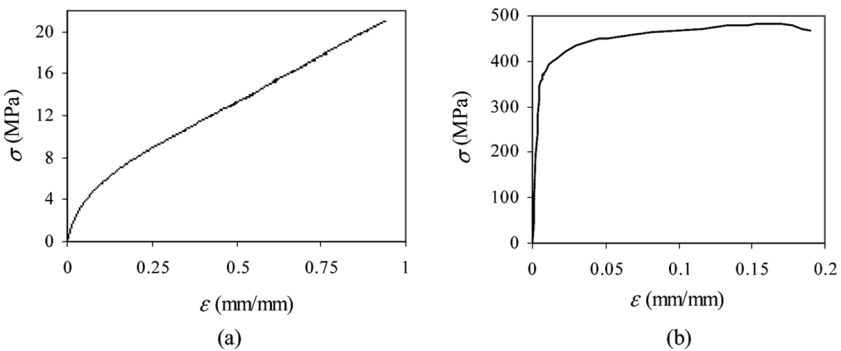
FIGURE 1 True tensile stress–strain behaviors of adhesive and adherend: (a) SBT 9244; (b) AA2024-T3 alloy.
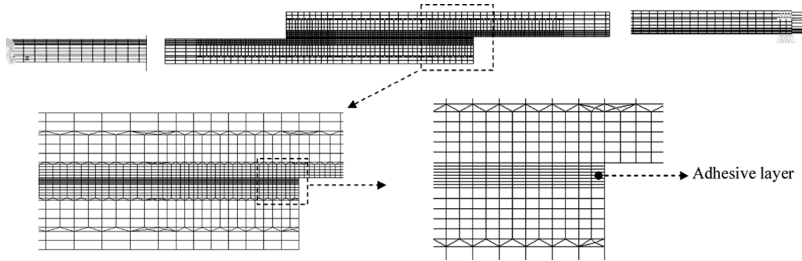
FIGURE 2 Mesh detail and boundary conditions for the SLJ with 12.5 mm overlap length and 1.6 mm adherend thickness.

package was utilized in this work [23]. The two-dimensional nonlinear finite element models of the SLJ geometry were generated with different adherend thickness/overlap length combinations and the geometrical parameters were the same as the experimental studies given in Table 3. Also, the stress analysis of SLJs was carried out according to the plane-strain assumption.

The mesh density can affect the accuracy of calculations. The smaller element size will generally give the higher maximum strain. Further dimension changes cause little effect when a specific size of finite elements is reached. For this reason, the size of elements in the mesh was reduced until a stable maximum strain value had been achieved. Consequently, eight elements through the adhesive thickness were used to model, and the number of elements was varied for every overlap length and adherend thickness. However, the mesh size was kept constant in all models [24]. The boundary conditions and mesh details considered in this study are represented in Figure 2.

4. RESULTS AND DISCUSSION

4.1. Experimental Results

The joints were tested in a Shimadzu universal testing machine (Shimadzu Corporation, Tokyo, Japan), equipped with a 50-kN load cell. The loading rate used was 5 mm/min, and the tests were carried out to failure at constant temperature and relative humidity (22°C and 50%, respectively). Four replicates were tested for all joint types.

Because of the large difference in the coefficients of thermal expansion between adhesive and adherend, residual thermal stresses are generated at adhesive–adherend interface during the curing process. These residual stresses can influence joint strength [5,30]. Considering that the strains occurring in adhesives at elevated temperatures

M. D. Aydın et al.

△ h=1.6 mm ○ h=3.2 mm □ h=4.8 mm   △ h=1.6 mm ○ h=3.2 mm □ h=4.8 mm

(a)   (b)
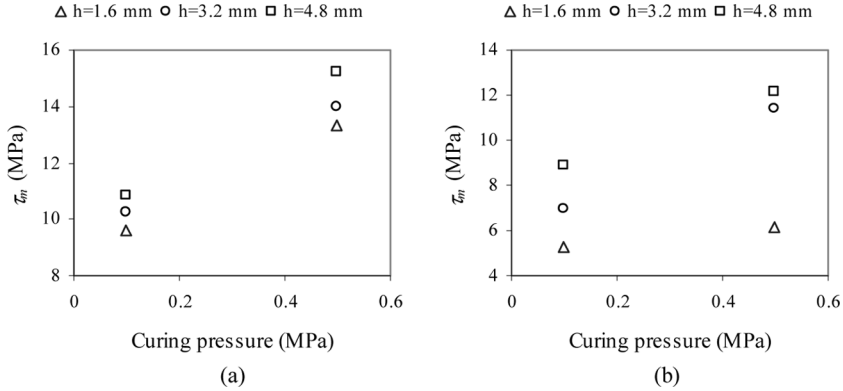
FIGURE 3 Effect of curing pressure on the mean strength (τ_m) of the joints: (a) SLJs with 1.6, 3.2, and 4.8 mm adherend thicknesses and only 25 mm overlap length; (b) SLJs with 1.6, 3.2, and 4.8 mm adherend thicknesses and only 100 mm overlap length.

are higher than those occurring at low temperatures, the magnitude of these stresses increases when the pressure is applied for the curing operation. Figure. 3 and Table 4 show the effect of curing pressure

**TABLE 4** Experimental and Predicted Failure Loads for SLJs

Adherend thickness h (mm)	Overlap length l (mm)	$P_{0.1}$ (N)	$P_{0.5}$ (N)	Failure type for SLJs with SBT 9244	P^* (N)	P_{FM} [27] (N)
1.6	12.5	—	4572 ± 103	Type I	3523.5	—
	25	5996.7 ± 404	8330 ± 584	Type II	6480	—
	50	—	14505 ± 312	Type III	12352.5	15435
	100	13106.7 ± 211	15421.7 ± 430	Type III	16200	15895
3.2	12.5	—	4545.6 ± 223	Type I	3360	—
	25	6396 ± 418	8758.7 ± 188	Type I	6400	—
	50	—	17546 ± 150	Type II	12000	—
	100	17470 ± 451	28506 ± 510	Type III	17600	30655
4.8	12.5	—	4554 ± 44	Type I	3600	—
	25	6780 ± 219	9506 ± 585	Type I	6960	—
	50	—	18526 ± 456	Type I	13200	—
	100	22256 ± 306	30441 ± 289	Type II	21000	39613

Notes. $P_{0.1}$: Experimental failure load for SLJs with SBT9244 curing at 0.1 MPa; $P_{0.5}$: experimental failure load for SLJs with SBT 9244 curing at 0.5 MPa; P^*: failure load predicted from FEA for SLJs with SBT9244; P_{FM}: experimental failure load for SLJs with FM 73.

on the load carried by the SLJ bonded with the flexible adhesive. It is clearly seen from these figures that the failure load of the joints increased when the curing pressure increased. For example, the average load capabilities of the SLJs with 4.8 mm adherend thickness and 25 mm overlap length cured under 0.5 MPa is 9506 N, which is 40.2% higher than that of the SLJs with the same adherend thickness and overlap length cured under 0.1 MPa as listed in Table 4.

On the other hand, the effects of overlap length and adherend thickness on failure load in the SLJs with SBT are shown in Figures 4a and 4b, respectively. When these figures are examined together with Table 4, it is seen that the increase in overlap length causes an increase in the load carried by the SLJ (Figure 4a). Although there is no effect of the adherend thickness on the strength of the SLJs with short overlap lengths (12.5 and 25 mm), there is an effect of the adherend thickness on the strength of the joints with long overlap lengths (50 and 100 mm) (Figure 4b). This situation is pertinent to the high-load-transfer capacity of the flexible adhesive, due to its high strain to failure, which enables the applied load to be carried by more area of the overlap and the joint to be stronger [24].

In the following, the plastic deformations and peel effect occurring in SLJs with SBT 9244 are compared with those occurring in the SLJs with FM 73 in another study made by Aydin *et al.* [27], to explain better the mechanical behavior of SBT 9244. In the study mentioned previously, the SLJs were made of AA2024-T3 aluminum plate bonded with a film-type adhesive FM 73 (produced by Cytec, Ostringen, Germany). The results from SLJs with 1.62, 3.2, and 4.8 mm adherend
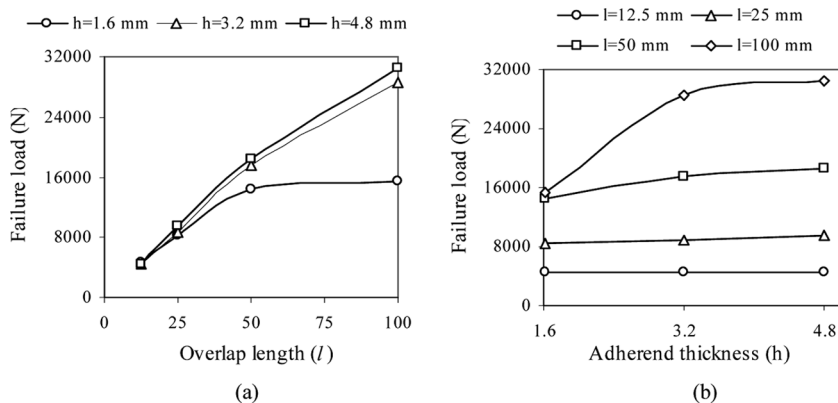

FIGURE 4 Effects of overlap length and adherend thickness on the failure load of SLJs prepared under 0.5 MPa curing pressure.

thicknesses and 100 mm overlap length were used only for comparison (Table 4). More information on the study can be found in Refs. [20,27].

The ultimate strength of FM 73 is 3.544 times as high as that of SBT 9244 (Table 1). On the other hand, the strain capability of SBT 9244 is extremely high. If Table 4 is examined, it is seen that the SLJs with SBT 9244 cured under 0.5 MPa can carry a load similar to the SLJs with FM 73, especially on the long overlap lengths such as 50–100 mm. In general, the midpoints of the overlap in the SLJs carry lower loads than the free edges, and this reduces the performance of the joint. The high strain capability of a flexible adhesive such as SBT 9244 provides the transfer of more stresses from the ends of the overlap to the middle part of the overlap and results in an increase in the load carried by the SLJs with SBT 9244. Furthermore, the flexible adhesive layer handles the high strains and plastic deformations on the adherend material by reducing and distributing the peel stress, which greatly affects the performance. This case can be seen in Figure 5. Comparison of the results obtained from lap shear tests for the two specimens types with 1.62 mm adherend thickness and 100 mm overlap length (see Table 4), one of which is made of SBT 9244 and the other of FM 73, shows that axial extension on the adherends of the SLJ with FM 73 is larger, although both of them can carry about the same load (Figure 5a). Similarly, when the rotations in the free edges for two different specimen types are compared, more
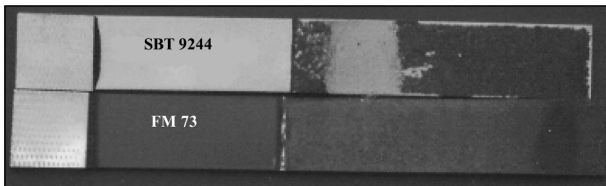
(a)
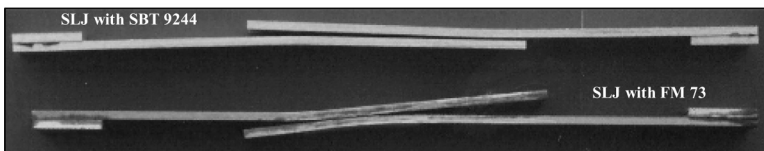
(b)

FIGURE 5 Two different SLJs with 100 mm overlap length and 1.6 mm adherend thickness, one of which is made with SBT 9244 and the other with FM 73: (a) the axial extension on the adherends of SLJs; (b) the rotations on the free edges for two different SLJs.

rotation exists on the free edges of the SLJ with FM 73 (Figure 5b). This is a very important situation in the case of the peel effect at the free ends of the overlap for the joints with SBT, considering that it causes initiation of a crack in this region when a critical value of the rotation angle at the free edges of overlap is reached.

Consequently, when all of the specimens tested are examined during lap shear test, the failure in SLJs with SBT according to adherend thickness and overlap length is of three different types, as follows (Table 4):

- *Type I*: Peel effect and any plastic deformation in the adherends were not observed. Failure in the joint was catastrophic without observing any initiation of a crack (fast fracture).
- *Type II*: Peel effect and plastic deformation in the adherends were observed. Failure in the joint was catastrophic without observing any initiation of a crack (fast fracture).
- *Type III*: Peel effect in the free ends of the overlap and large plastic deformation in the adherends were strongly marked. At the free ends of the overlap, the initiation of a crack was observed, and then, the cracks at both free ends moved to the center of the overlap (slow tearing) and catastrophic failure occurred when a specific failure zone length at the center of the overlap was reached.

An important point to be considered is that the increase in adherend thickness causes an increase in Type I, failure due to the changing relative stiffnesses (See Table 4). Also, the failure occurs within the adhesive layer and is partly cohesive and ductile but very close to the adherend–adhesive interface. Finally, it can be concluded that interfacial bond failure occurs in the joints (Figure 6).

4.2. FE Analysis Results and Comparison with Experimental Results

To predict the failure load, the ultimate strength (σ_t) of the adhesive given in Table 1 was used, and the adhesive was assumed to fail when the Raghava equivalent stress (σ_{eq}) calculated at any point in the adhesive layer reaches the ultimate strength (σ_t) of the adhesive.

The finite-element solution that considers nonlinear material behavior is reached by dividing the total load in steps to track the equilibrium paths and iterating to a converging solution at each load increment. In the study, the number of load steps for each joint type changed as a result of changing predicted failure loads. Hence, a load
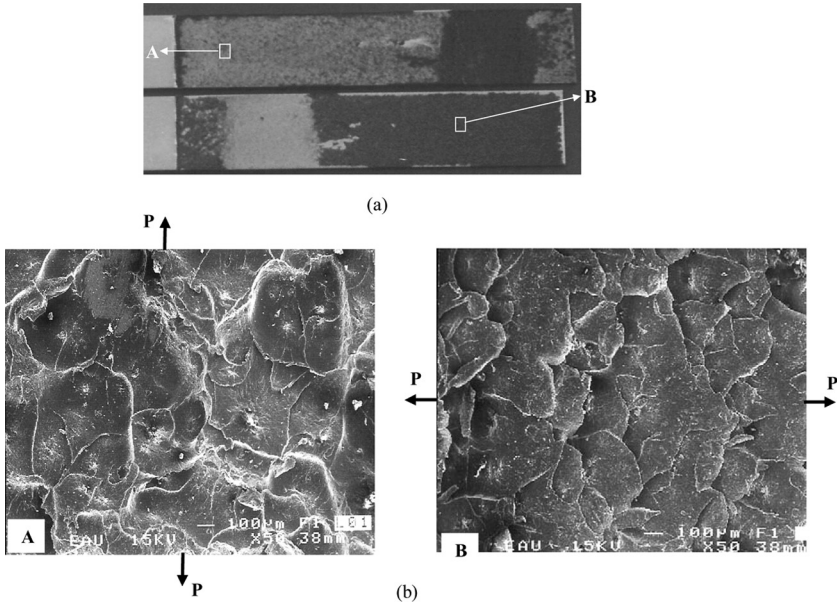
FIGURE 6 (a) Fracture surfaces from SLJ curing at 0.5 MPa and with 100 mm overlap length; (b) SEM images from points A and B.

of 5 N per mm width at each load step was applied for all joint types. The remaining load was then applied in the last step.

The results predicted from FEA and obtained experimentally are shown in Table 4. The results predicted from FEA did not converge to the average experimental failure load of the SLJs cured under 0.5 Mpa, whereas the results predicted from FEA converged to the average experimental failure loads of the SLJs cured under 0.1 MPa. The residual thermal stresses generally occur because of different thermal properties between the adhesive and the adherend during the curing process at elevated temperatures [5,19]. The importance of these stresses will increase when the pressure applied for curing of the adhesives is taken into consideration [20]. For this reason, in addition to other parameters such as the dependence on strain rate and the lack of yield criteria of adhesives, it can be said that the residual thermal stresses occurring as a result of the applied pressure during the curing process at elevated temperature need to be taken into consideration so as to simulate accurately the mechanical behavior of adhesively bonded joints. In practice, the magnitude of these stesses is difficult to predict. Therefore, more detailed investigation,

which comprises the mechanical and thermal properties of adhesives at different temperatures, needs to be performed to explain the effect of curing pressure on the strength of adhesively bonded joints.

The present FE analysis results have shown that the most critical points are along the adherend–adhesive interfaces, and the maximum peel (σ_y) and shear (τ_{xy}) stresses are located between the centerline and the adherend–adhesive interfaces and at the opposite corner ends of overlap (points A and C or around points A and C as seen in the figure in Table 3). For this reason, the line A–B on the adhesive side was
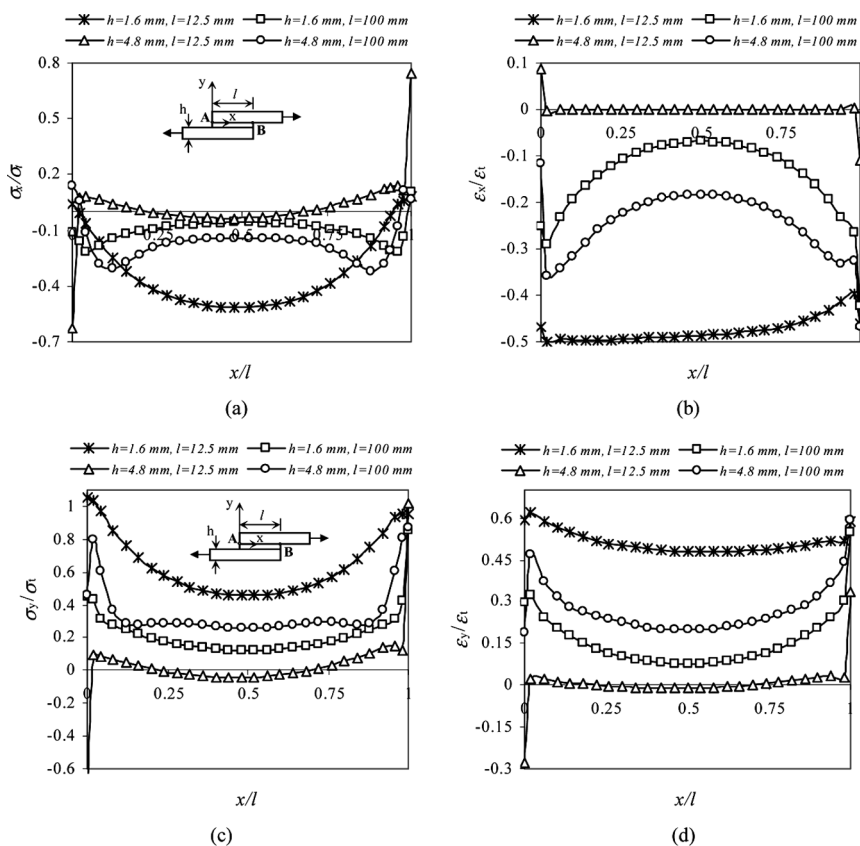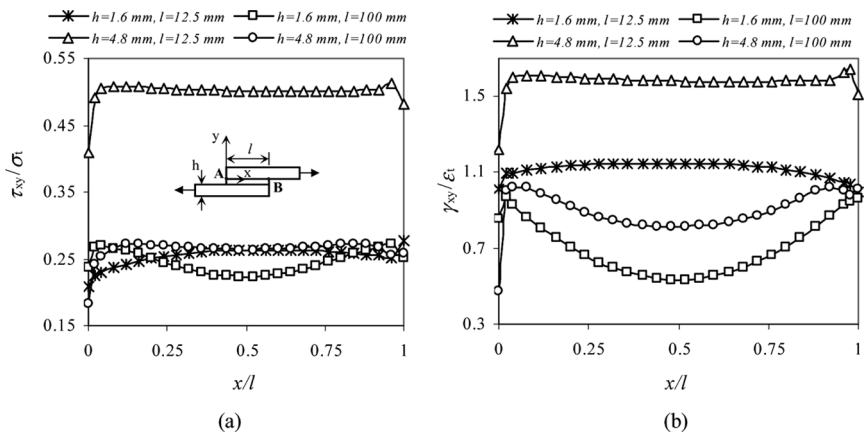

FIGURE 7 Normal stress and strain distributions along the line A–B on the adhesive side for the SLJs with 12.5 and 100 mm overlap length and 1.6 and 4.8 mm adherend thickness: (a) normalized σ_x stress distributions; (b) normalized ε_x strain distributions; (c) normalized σ_y stress distributions; (d) normalized ε_y strain distributions.

taken into consideration for the stress analyse (see figure in Table 3) and all of the stress (σ_x, σ_y, τ_{xy}, and σ_{eq}) and strain (ε_x, ε_y, γ_{xy}, and ε_{eq}) distributions were normalized by dividing by the ultimate strength (σ_t) and strain (ε_t) of the adhesive (Figures 7–9).

The distributions of normal stresses (σ_x, σ_y) and strains (ε_x, ε_y) along the line A–B on the adhesive side obtained from FE analyses are presented in Figure 7. The peak tensile peel stress and strain values occur in the left free edge of the adhesive layer–lower adherend interface and in the right free edge of the adhesive layer–upper adherend interface. When the magnitude of shear (τ_{xy}), longitudinal (σ_x), and peel (σ_y) stresses (Figures 7a, 7c, and 8a) are considered, it is clearly seen that the high peel stress distributions have a very important influence on the initiation and propagation of failure at the free edges of the overlap.

Figure 8 indicates that more shear stress and strain are transferred from the end to the center of the overlap with increasing adherend thickness, due to the reduced plastic deformations of the adherends. Therefore, the effect of shear stresses on the failure and strength of the adhesively bonded joints increases. Similarly, it is evident that more equivalent stress and strain are transferred from the end to the center of the overlap with increasing adherend thickness, as seen from Figure 9. This is the reason for increase in the strength of joints with increasing adherend thickness at the same overlap length.

FIGURE 8 Shear stress and strain distributions along the line A–B on the adhesive side for the SLJs with 12.5 and 100 mm overlap length and 1.6 and 4.8 mm adherend thickness: (a) normalized τ_{xy} stress distributions; (b) normalized γ_{xy} strain distributions.
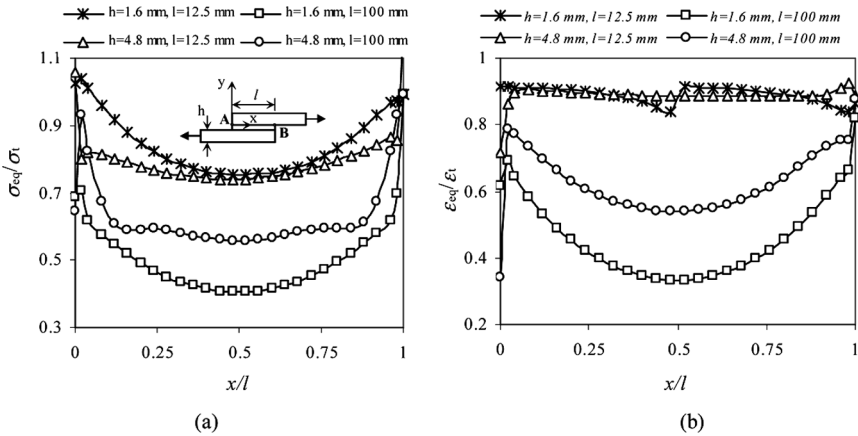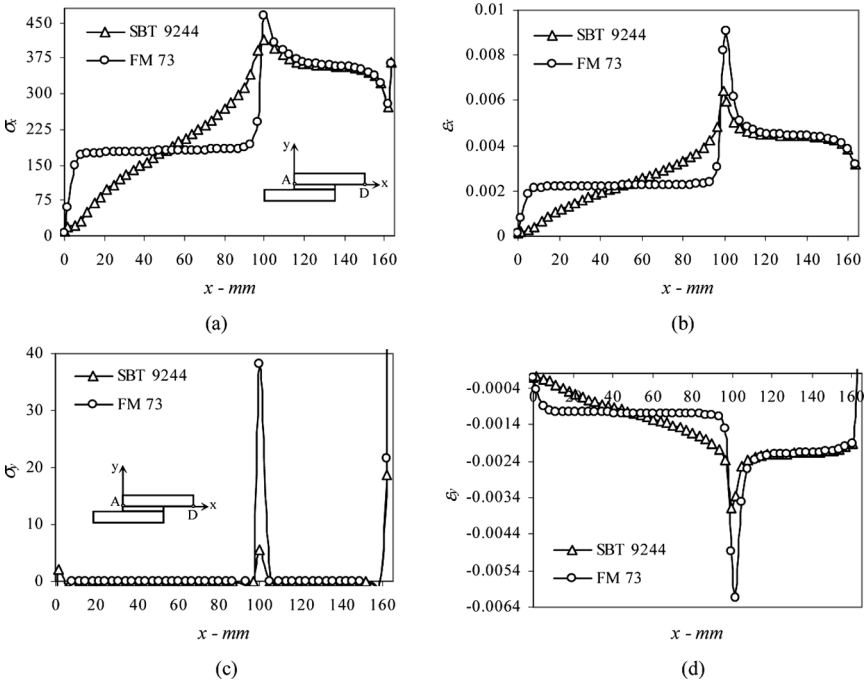
FIGURE 9 Equivalent stress and strain distributions along the line A–B on the adhesive side for the SLJs with 12.5 and 100 mm overlap length and 1.6 and 4.8 mm adherend thickness: (a) normalized σ_{eq} stress distributions; (b) normalized ε_{eq} strain distributions.

On the other hand, nonlinear FEA was carried out on the joint with FM 73 for only 1.6 mm adherend thickness and 100 mm overlap length under the same mesh, load, and boundary conditions applied to the SLJ with SBT9244 (see Figure 2), to explain better the effects of the rotation produced by peel stress on the free ends of the SLJ and the plastic deformations of the adherends. Thus, the stress and strain distributions along the line A–D on the bottom of the upper adherends of the SLJs with both SBT 9244 and FM 73 are compared in Figures 10–12 for a nominal axial load applied per unit width of 540 N/mm.

The results of analysis indicate that for the same load level, the maximum values of the stresses and strains are lower for the SLJ with SBT, especially in the free edges of the overlap (Figures 10–12).

As observed for the normal and shear strain components along the line A–D on the upper adherends (Figures 10b, 10d, and 11b), ε_x, ε_y, and γ_{xy} strain distributions are higher for the joints with FM 73. This means that more rotation and axial extension exist on the adherends of the SLJ with FM 73 with respect to the adherend of the SLJ with SBT (Figure 5). Similarly, when the von Mises equivalent stress and strain distributions are examined together with the experimental results mentioned previously (Figure 12), it is clearly shown that the flexible adhesive layer handles the high strains and plastic deformations of the adhered material. This situation provides an important increase in the performance of the joint with SBT.
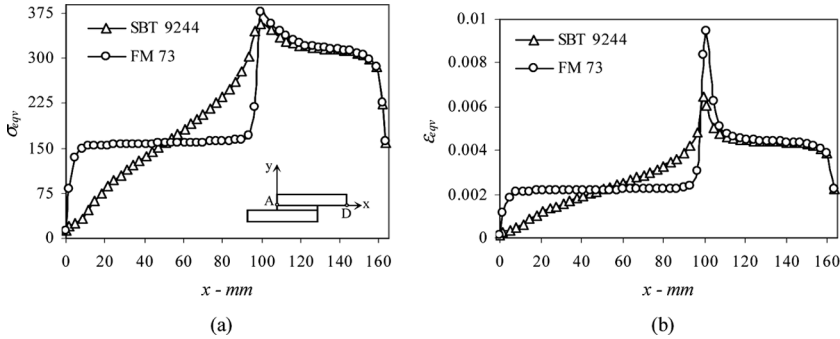
FIGURE 10 Normal stress and strain distributions along the line A–D on the adherends for the SLJs with 100 mm overlap length and 1.6 adherend thickness, one of which is made with SBT 9244 and the other with FM 73: (a) σ_x stress distributions; (b) ε_x strain distributions; (c) σ_y stress distributions; (d) ε_y strain distributions.
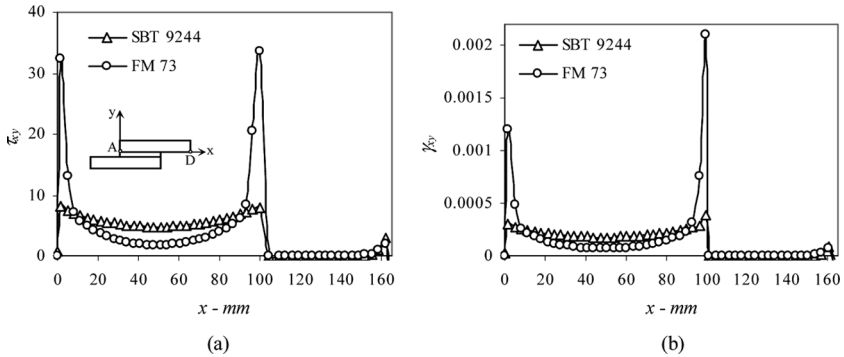
FIGURE 11 Shear stress and strain distributions along the line A–D on the adherends for the SLJs with 100 mm overlap length and 1.6 adherend thickness, one of which is made with SBT 9244 and the other with FM 73: (a) τ_{xy} stress distributions; (b) γ_{xy} strain distributions.

FIGURE 12 von Mises equivalent stress and strain distributions along the line A–D on the adherends for the SLJs with 100 mm overlap length and 1.6 adherend thickness, one of which is made with SBT 9244 and the other with FM 73: (a) σ_{eqv} stress distributions; (b) ε_{eqv} strain distributions.

Consequently, crack initiation will probably occur at points A and C or around points A and C (see figure in Table 3) within the adhesive layer. Then, the cracks at both free ends progress to the center of overlap before joining each other. The propagation across the bond thickness would consist of a mixed failure mode of shear and peel due to the combined out of-plane and in-plane shear stress.

5. CONCLUSIONS

This study has dealt with the effect of the curing pressure on predicting of the failure load of adhesively bonded joints *via* a non-linear finite element method. The results obtained are as follows:

- It can be stated that the failure in SLJs with SBT according to adherend thickness and overlap length occurs in three different types and, also, an important point to be considered is that the increase in adherend thickness causes an increase in *Type I* failure.
- In addition to other parameters such as the dependence on strain rate or the lack of yield criteria of adhesives, due to hydrostatic sensitivity, the residual thermal stresses occurring due to the curing pressure at elevated temperature need to be taken into account in order to simulate accurately the mechanical behaviors of adhesively bonded joints.
- The effect of shear stresses on the failure and strength of the adhesively bonded joints increases with the increase of the adherend thickness.

- It is evident that more equivalent stress and strain are transferred from the end to the center of the overlap with increasing the adherend thickness. This is the reason for the increase in the strength of the joints with increasing adherend thickness at the same overlap length.
- The flexible adhesive layer undertakes the high strains and plastic deformations on the adhered material by reducing and distributing the peel stress which greatly affects the performance of joints.

REFERENCES

[1] Dean, G. D. and Crocker, L. E., *Comparison of the Measured and Predicted Deformation of an Adhesively Bonded Lap-Joint Specimen*, NPL CMMT(A) 293 (National Physical Laboratory, Teddington, UK, 2000).

[2] Read, B. E., Dean, G. D., and Ferriss, D. H., *An Elastic–Plastic Model for the Nonlinear Mechanical Behaviour of Rubber-Toughened Adhesives,* NPL CMMT(A) 289 (National Physical Laboratory, Teddington, UK, 2000).

[3] Broughton, W. R., Crocker, L. E., and Urquhart, J. M., *Strength of Adhesive Joints: A Parametric Study*, NPL MATC(A) 27 (National Physical Laboratory, Teddington, UK, 2000).

[4] Dean, G. D., Crocker, L. E., Read, B., and Wright, L., *Int. J. Adhes. Adhes.* **24**, 295–306 (2004).

[5] Adams, R. D., Coppendale, J., Mallick, V., and Al-Hamdan, H., *Int. J. Adhes. Adhes.* **12**(3), 185–190 (1992).

[6] Wang, C. H. and Chalkley, P., *Int. J. Adhes. Adhes.* **20**(2), 155–164 (2000).

[7] Adams, R. D., *The Mechanics of Bonded Joints Structural Adhesives in Engineering* (ImechE Conference Publications, Suffolk, UK 1986).

[8] Harris, J. A. and Adams, R. D., *Int. J. Adhes. Adhes.* **4**(2), 65–78 (1984).

[9] Crocombe, A. D., *Int. J. Adhes. Adhes.* **15**(1), 21–27 (1995).

[10] Zgoul, M. and Crocombe, A. D., *Int. J. Adhes. Adhes.* **24**(4), 355–366 (2004).

[11] Adams, R. D. and Harris, J. A., *Int. J. Adhes. Adhes.* **7**(2), 69–80 (1987).

[12] Pires, I., Quintino, L., Durodola, J. F., and Beevers, A., *Int. J. Adhes. Adhes.* **23**(3), 215–223 (2003).

[13] Harrison, N. L. and Harrison, W. J., *J. Adhes.* **3**, 195–212 (1972).

[14] Cho, D. H. and Lee, D. G., *J. Adhes. Sci. Technol.* **14**, 939–963 (2000).

[15] Kim, Y. G., Lee, S. J., Lee, D. G., and Jeong, K. S., *J. Adhes.* **60**, 125–140 (1997).

[16] Kim, Y. G. and Lee, D. G., *J. Adhes.* **65**, 163–185 (1998).

[17] Cho, J. H., Kong, D. I., Park, C. E., and Jin, M. Y., *J. Adhes. Sci. Technol.* **12**(5), 507–521 (1998).

[18] Humfeld, G. R. and Dillard, D. A., *J. Adhes.* **65**, 277–306 (1998).

[19] Kim, J. K. and Lee, D. G., *J. Adhes. Sci. Technol.* **18**, 87–107 (2004).

[20] Aydm, M. D., *Experimental and Theoretical Investigation of Mechanical Properties of the Adhesive Bonded Single Lap Joint*, PhD Thesis, University of Atatürk, Turkey (2003).

[21] Drucker, D. C. and Prager, W., *Q. Appl. Math.* **10**, 157–165 (1952).

[22] Raghava, R. S., Cadell, R. M., and Yeh, G. S., *J. Mater. Sci.* **8**, 225–232 (1973).

[23] ANSYS®, The General Purpose Finite Element Software (Version 10.0) (Swanson Analysis Systems, Inc., Houston, Texas, 2006).

[24] Aydin, M. D., Özel, A., and Temiz, Ş., *J. Adhes. Sci. Technol.* **18**(14), 1589–1602 (2004).
[25] Kadioglu, F. and Adams, R. D., *J. Adhes. Sci. Technol.* **16**(2), 179–195 (2002).
[26] Kadioglu, F., Vaughn, L. F., Guild, F. J., and Adams, R. D., *J. Adhes.* **78**(5), 355–381 (2002).
[27] Aydın, M. D., Özel, A., and Temiz, Ş., *J. Adhes. Sci. Technol.* **19**(8), 705–718 (2005).
[28] Chiu, W. K., Chalkley, P. D., and Jones, R., *Comput. Struct.* **53**, 483–489 (1994).
[29] Chun, H. W. and Chalkley, P. D., *Int. J. Adhes. Adhes.* **20**, 155–164 (2000).
[30] Ramani, K. and Zhao, W., *Int. J. Adhes. Adhes.* **17**(4), 353–357 (1997).